Characterization and Application of Nanomaterials 2024, 7(2), 4768.
https://doi.org/10.24294/can.v7i2.4768

Article

Non-enzymatic detection of 17β-estradiol in real samples using PANI@CeO_2 nanocomposite

Aditya Dam, Tanu Rajput, Sakshi Verma, Devendra Kumar*

Department of Applied Chemistry, Delhi Technological University, Delhi 110042, India
*** Corresponding author:** Devendra Kumar, dkumar@dce.ac.in

CITATION

Dam A, Rajput T, Verma S, Kumar D. Non-enzymatic detection of 17β-estradiol in real samples using PANI@CeO_2 nanocomposite. Characterization and Application of Nanomaterials. 2024; 7(2): 4768. https://doi.org/10.24294/can.v7i2.4768

ARTICLE INFO

Received: 20 February 2024
Accepted: 22 July 2024
Available online: 19 August 2024

Abstract: Herein, we developed a non-enzymatic biosensing platform using polyaniline (PANI) polymer matrix grafted with CeO_2. The one-pot synthesized nanocomposite has been used for the detection of 17β-estradiol (E2). The homogeneous distribution of CeO_2 onto the PANI matrix leads to an increase in surface area, conductivity, and effectiveness of the synthesized nanocomposite PANI@CeO_2. The PANI@CeO_2 nanocomposite was characterized using structural and morphological techniques. Further, the electrode fabrication was performed electrophoretically by depositing the PANI@CeO_2 nanocomposite onto the ITO electrode. The PANI@CeO_2/ITO showed enhanced electrochemical behavior as compared to PANI/ITO. Detection of E2 was carried out using the differential pulse voltametric technique (DPV). Linearity has been observed through the detection range of 1 µM–100 µM with LOD = 2.15 µM. The developed biosensor has been found to be stable and selective towards E2. It has been successfully utilized for the detection of E2 in real samples like tap water and human urine samples. Thus, this research encourages its use for more applications in clinical diagnosis and biomedical sciences.

Keywords: polyaniline; 17β-estradiol; biosensor; tap water; urine; CeO_2

1. Introduction

The excessive use of steroid growth hormones has resulted in the widespread presence of 17β-estradiol (E2) in food commodities such as meat and dairy products. These hormones are excreted by animals into the environment, serving as prevalent forms of environmental endocrine disruptors [1]. At low concentrations, the abuse of steroid growth hormones can mimic the effects of female sex hormones in the human body and disrupt hormone actions through different mechanisms. This interference with the endocrine system can lead to adverse effects such as infertility, diabetes, birth defects, PCOD, and reproductive dysfunctions in humans. Exceeding a certain threshold concentration, exogenous E2 can disturb the balance within the human body. It has been reported that elevated levels of E2 lead to an increased incidence of prostate cancer in men and breast cancer in women [2,3].

During the last decade, many analytical methods have been reported for the determination of E2, such as HPLC, LC-MS, GC-MS, etc. These methodologies use expensive instruments, require intricate operation, extended assay time, and personnel with specialized training. Some alternative methods that have been introduced for detecting E2 are surface plasmon resonance biosensors, surface molecular imprinting techniques, colorimetric methods, and enzyme-linked immunosorbent assays. Despite the appreciable sensitivity of these newly developed methods for detecting E2, most of them still require expensive instruments, similar to

chromatography techniques. As a result, they are not suitable for on-site detections due to cost and instrument dependency limitations [4–6]. Also, the detection of hormones based on enzyme immobilization mobility is gaining popularity due to its high selectivity, easy fabrication, and rapid response. Despite this popularity, this technique comes with various limitations, like high cost, low sensitivity, and leaking of enzyme from the transducer surface. Therefore, there is a strong demand for reliable, rapid, and user-friendly biosensors that can effectively detect low concentrations of E2 in samples [7,8].

Conducting polymers (CP) due to their electrochemical activity, mechanical elasticity, biocompatibility, electrical conductivity, and environmental stability are the most liable to be used as sensing elements in analytical and bioanalytical systems. Electrochemical biosensors based on enzymatic and non-enzymatic methods have gained tremendous attention throughout the world. However, enzymatic methods are known to have some drawbacks, such as thermal and storage stability, environmental selectivity, etc. [9,10]. Hence, scientists have been more focused on the development of non-enzymatic biosensors in the last decade because of their high selectivity and lower cost than enzymatic ones. The most common among them is the MIP-based sensors, which do not require any biologically recognized element. The principle for these nonenzymatic biosensors for the detection of E2 is based on the direct oxidation of the hydroxyl group. The sensing properties of CP's can be modified by alternating their surface and morphology, such as by developing a metal-based structure grafted with conducting polymer. N-type inorganic semiconductors such as CeO_2, ZnO, TiO_2, and WO_3 can be used efficiently with conducting polymers as a sensing material [11,12].

Polyaniline (PANI) displays exceptional advantages, including easy synthesis, superior electrical conductivity, and reversible redox behavior. Despite the numerous positive characteristics of the polymer, PANI-based chemical sensors can face limitations in terms of sensitivity, linearity, selectivity, or stability. One way to overcome these limitations is by incorporating a secondary material into the PANI, resulting in the formation of a polymeric composite. The integration of PANI with a secondary nanocomponent, such as metallic nanoparticles, metal oxide nanoparticles, carbon compounds, or polymers, leads to enhanced functionality and improved performance, providing an effective design approach [13,14]. The synergistic interactions between the constituents in nanocomposites of PANI and metal oxides such as CeO_2 result in improved properties, making them highly valuable for applications such as sensors and biosensors, photovoltaics, and batteries. Nanocomposites of PANI with CeO_2 have been extensively explored for sensing applications. The enhanced sensor response of these composites can be attributed to the formation of electron-conducting pathways within the material, leading to improved device efficiency. The inclusion of semiconductor metal oxide CeO_2 into polymer matrices PANI has been shown to improve the mechanical, thermal, dielectric, and optical properties of polymers, enabling high carrier mobilities [15]. This research work reveals the biosensory fabrication of electrodes using synthesized PANI@CeO_2 nanocomposite, which acts as an effective sensing platform for E2 detection (**Figure 1**). The performance of PANI@CeO_2 composite as a sensing platform has been analysed in real samples, i.e., human urine and tap water.

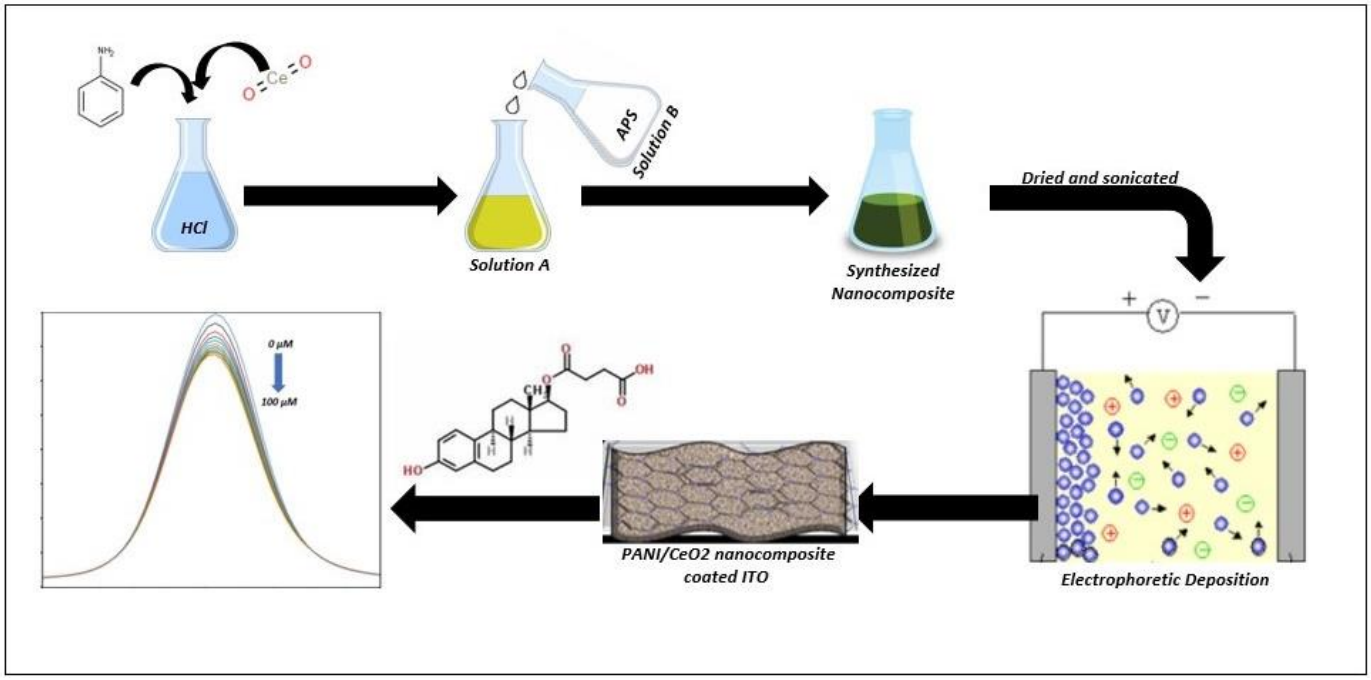

Figure 1. Schematic diagram of the synthesis of PANI@CeO_2 and its deposition on ITO.

2. Materials and methods

2.1. Materials required

For synthesizing the PANI, CeO_2, and PANI@CeO_2 nanocomposite, we used aniline and ammonium persulfate, bought from Central Drug House (Pvt), [$Ce(NO_3)_3 \cdot 6H_2O$], 99% trace metal basis, procured from Sigma Aldrich (France), hydrochloric acid (HCl, 25%), and liquor ammonia (25% ammonia) procured from Thermofisher Scientific, India. Other chemicals, i.e., di-sodium hydrogen orthophosphate dihydrate, potassium ferrocyanide, sodium dihydrogen orthophosphate, and potassium ferricyanide, were purchased from Qualigens Fine Chemicals for preparing PBS and Ferro-Ferri solution (pH = 7.4). The cleaning was done using 100% acetone and 99.9% ethanol, which were purchased from central drug house (Pvt).

2.2. Synthesis of polyaniline

For the synthesis of PANI, we took 1 mL aniline and mixed it with 15 mL HCl (1 M) to get solution-A. Then solution B was prepared by dissolving ammonium persulfate in 15 mL HCl (1 M). The molar ratio of aniline with respect to ammonium persulfate was taken to be 1:1.15, respectively. In an ice bath maintaining 0–5 °C, solution-b was added dropwise into solution-a, followed by 3 h of stirring under the same condition. At last, the resultant solution was kept overnight in the refrigerator and rinsed with acetone and distilled water the next day to remove impurities. The obtained product was then left to dry in an oven at 60 °C to get dark green-colored PANI [16].

2.3. Synthesis of CeO_2

For the preparation of CeO_2 nanoparticles, 1.5 m mol of Cerium (III) nitrate hexahydrate was dissolved in distilled water (50 mL) with the addition of 1.5 mL of liquid ammonia. The resulting solution was stirred for around 30 min using a magnetic stirrer. Following this, the solution mixture was shifted to an autoclave (120 mL) (Teflon-lined stainless steel) and left at 180 ℃ in an oven for 24 h. The obtained stagnant was then cooled at room temperature, rinsed with both distilled water and ethanol repeatedly for the excretion of excessive ammonium hydroxide, and left at 60 ℃ for 24 h to get the dry, desired pale-yellow, white-colored product.

2.4. Synthesis of PANI@CeO_2 nanocomposite

For synthesis of PANI@CeO_2 nanocomposite, 40% (w/w) of synthesized CeO_2 was mixed with 1 mL of aniline in 15 mL of HCl (1 M) to get solution-a, followed by the same procedure as mentioned in Synthesis of PANI.

2.5. Electrophoretic deposition (EPD) on electrode

A GX300C (Genetix) electrophoretic unit was used to carry out the process of electrophoretic deposition, where platinum was used as the counter electrode. We deposited all three synthesized compounds on an ITO (indium tin oxide) coated glass electrode. For that, we mixed 1 mg of each compound with 10 mL of distilled water separately and ultrasonicated them for 3–4 h. The EPD process was conducted at a constant voltage of 10 V provided via a DC power supply for stable and efficient deposition and optimized at 7 s for PANI and cerium (IV) oxide suspension, and for PANI@CeO_2 nanocomposite suspension, it was optimized at 15 s. After EPD, the electrodes were removed from the suspension and stored in a refrigerator for further use.

2.6. Characterization

For the study of X-ray diffraction of the synthesized materials, Cu Kα radiations with a wavelength of λ = 1.5406 Å based on a Bruker D-8 Advance X-ray diffractometer (XRD) have been used. For the study of the presence of functional groups and saturation in materials, the Perkin Elmer Fourier transform infrared (FTIR) spectrum (model spectrum 2) has been used. We used a Zeta potential analyzer (Malvern Instruments Ltd.) for analysing the charge of the materials. TGA 4000, PerkinElmer, was used in the range of 0–600 ℃ in an atmosphere of nitrogen with a constant heating rate of 10 ℃/min for studying the degradation of materials with temperature. Similarly, DSC 8000, Perkin Elmer, was used for differential scanning calorimetry for the analysis of thermal characteristics. For electrochemical studies, we used autolab potentiostat/galvanostat (Eco-Chemie, the Netherlands), which is a three-electrode cell having ITO, platinum, and Ag/AgCl as a working, inert, and auxiliary electrode in phosphate buffered saline (PBS; pH 7.4; 100 mM) mixed with ferrocyanide and ferricyanide $[Fe(CN)_6]^{3-/4-}$ of 5 mM concentration each.

3. Results and discussion

3.1. X-ray diffraction study

The powder XRD pattern of CeO_2 and PANI@CeO_2 nanocomposite and PANI has been shown in **Figure 2A** and **Figure S1**. It has been observed that CeO_2 shows clearly distinct XRD peaks at 2θ = 28.5°, 33.1°, 47.7°, 57.1°, 59.3°, 69.6°, 77.0° and 79.2° respectively. No other peaks are obtained, which indicates the successful synthesis of CeO_2. The observed X-ray patterns of the synthesized CeO_2 satisfied the fluorite-type crystal cubic phase of CeO_2 (JC-PDS card no 01-075-8371) [17].

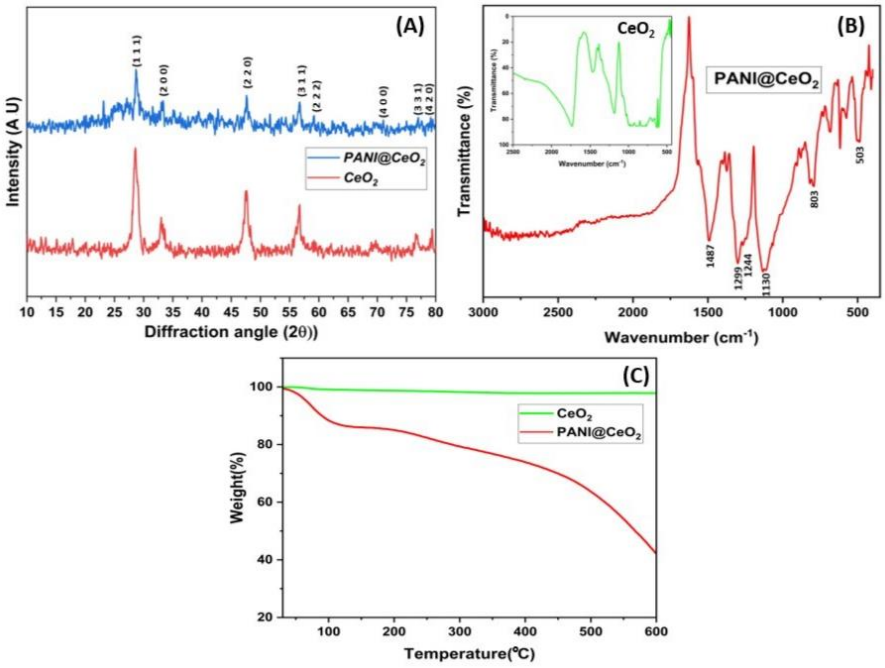

Figure 2. (A) XRD spectra; **(B)** FT-IR spectra; **(C)** TGA plot of PANI@CeO_2 and CeO_2.

The results here indicate that both the compounds maintained its characteristic in the composite mixture.

In the XRD pattern of PANI@CeO_2 nanocomposite, it was observed that the diffraction peaks of PANI and CeO_2 overlapped with each other. Both the PANI and PANI@CeO_2 nanocomposite show a wide peak located at 2θ = 26° satisfying the amorphous (semi-crystalline) nature of PANI. The synthesized PANI@CeO_2 nanocomposite shows its peaks at 2θ = 28.5°, 33.1°, 47.7°, 57.1°, 59.3°, 69.6°, 77.0° and 79.2° respectively which resembled the (111), (200), (220), (311), (222), (400), (331) and (420) Bragg's crystal plane reflections [18].

3.2. Fourier transform infrared study

The FTIR spectra of CeO_2, PANI@CeO_2 nanocomposite, and PANI are shown in **Figure 2B** and **Figure S2**. The vibration peaks of the as-prepared PANI@CeO_2 nanocomposite sample appear at 503, 689, 803, 1130, 1299, 1244, 1487, and 2822 (cm^{-1}). The C–N stretching of a secondary aromatic amine is responsible for a minor, distinct peak observed at 1299 cm^{-1}. The wide and sharp peaks at 1130 cm^{-1}

correspond to the bending vibration of C–H. The very small and clear peaks at 803 cm^{-1} indicate the metal-oxygen bands. The minor peak at 1244 cm^{-1} showed the C–N stretching and C–C stretching bands of PANI. The sharp peak at 1487 cm^{-1} showed the Benzenoid ring stretching of PANI. The broad peak at 503 cm^{-1} corresponds to the metal-oxygen stretching frequency. As the percentage of CeO_2 in the PANI@CeO_2 composite increases, the intensity also increases. For pure CeO_2 this peak was observed at 496 cm^{-1}, and moved at 503 cm^{-1} in the case of PANI@CeO_2 which illustrates the weak interaction between CeO_2 and PANI, while other prominent peaks of pure CeO_2 are 619, 1126, 1356, and 1569 (cm^{-1}) attributes to the stretching band of the metal-oxygen bond [17,19–21].

3.3. Thermogravimetric analysis study

From the TGA of CeO_2 and PANI@CeO_2 as shown in **Figure 2C**, it is observed that pure CeO_2 crystals are superiorly stable and thermally resistant in the temperature range of 20–600 °C whereas PANI@CeO_2 nanocomposite shows a loss in its mass in two steps. The first decrease in mass of about 10% occurs in the range of 40–100 °C owing to the deprivation of water from PANI chains. In the second step, loss of mass occurs in the range of 250–600 °C, corresponding to the breaking of polymeric chains. It is observed that when the CeO_2 to aniline ratio is about 40% in the PANI@CeO_2 nanocomposite, it shows highest thermal stability. The higher the content of CeO_2 in the composite, the more strengthening occurs between the polymeric chains and CeO_2 and the thermal decomposition of the chains is restricted accordingly [22–24].

3.4. Morphological studies

The surface morphology of PANI and PANI@CeO_2 was analysed using scanning electron microscopy (SEM), as shown in **Figure 3A,B**, respectively. The morphology of PANI appeared as a grain-like structure that contains some pores and voids. From the morphology of PANI@CeO_2 nanocomposites, it was observed that PANI@CeO_2 has some spherical and irregularly shaped grains with diameters in the nanorange, where the CeO_2 nanoparticles are homogeneously compacted in the PANI matrix, leading to homogeneous morphology and the higher conductivity of PANI@CeO_2 nanocomposite.

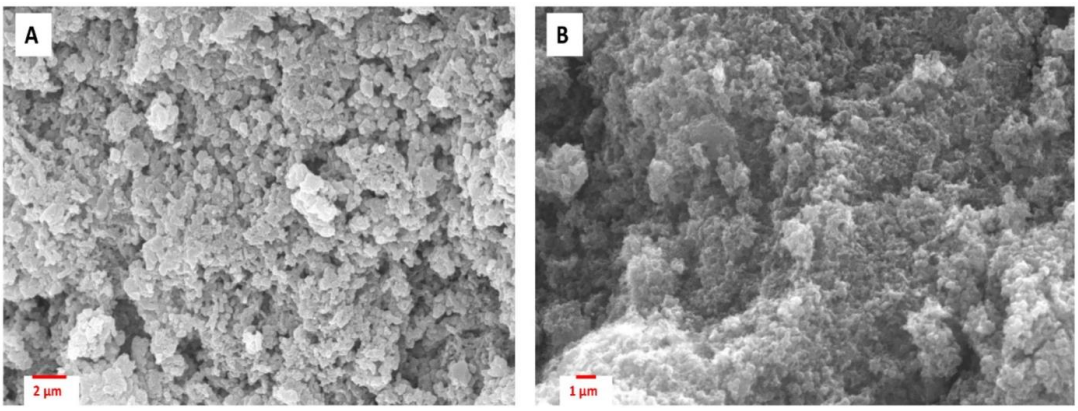

Figure 3. (A) SEM images of PANI; **(B)** SEM images of PANI@CeO_2 nanocomposite. Indicating more homogeneously compacted morphology of the nanocomposite.

4. Electrochemical studies

4.1. Electrochemical studies of electrodes

Electrochemical studies of the PANI/ITO and PANI@CeO_2/ITO electrodes have been performed using Cyclic Voltammetry (CV) technique in PBS (pH—7.4; 100 mM) carrying $[Fe(CN)_6]^{3-/4-}$ solution of 5 mM concentration. At 50 mV/s, it was noticed that PANI@CeO_2 electrode exhibits higher current with respect to the PANI/ITO electrode, which illustrates the better electron conduction ability of the PANI@CeO_2/ITO electrode (**Figure 4A**).

A scan rate study has also been performed for both electrodes, as shown in **Figure 4B** and **Figure S3**. It is observed that the anodic peak potential rises from 10 mV/s to 300 mV/s and the cathodic peak potential collapses with an increase in the scanning rate for both the PANI and PANI@CeO_2 modified ITO electrodes. This led to a linear relation between the cathodic and anodic peak potentials (E_{pa} and E_{pc}) of PANI and PANI@CeO_2 with respect to logarithmic scan rate (log$v$) (**Figure 4D**) [Equations (1)–(4)] [25].

A linear correlation between the cathodic and anodic peak currents (I_{pa} and I_{pc}) with respect to the square root of scan rates ($v^{1/2}$) has also been observed from the scan rate studies of PANI and PANI@CeO_2 grafted ITO electrodes (**Figure 4C**) and has been depicted by Equations (5)–(8).

$$E_{pa}\ [PANI@CeO_2/ITO]\ (V) = 0.04968 \log(v) + 0.148;\ R^2 = 0.9492 \quad (1)$$

$$E_{pc}\ [PANI@CeO_2/ITO]\ (V) = -0.0708 \log(v) + 0.183;\ R^2 = 0.9710 \quad (2)$$

$$E_{pa}\ [PANI/ITO]\ (V) = 0.1075 \log(v) + 0.1187;\ R^2 = 0.9833 \quad (3)$$

$$E_{pc}\ [PANI/ITO]\ (V) = -0.2257 \log(v) + 0.3403;\ R^2 = 0.8701 \quad (4)$$

$$I_{pa}\ [PANI@CeO_2/ITO]\ (A) = 2.75 \times 10^{-5} \times v^{1/2} + 4.483 \times 10^{-5};\ R^2 = 0.994 \quad (5)$$

$$I_{pc}\ [PANI@CeO_2/ITO]\ (A) = -1.77 \times 10^{-5} \times v^{1/2} - 7.008 \times 10^{-5};\ R^2 = 0.978 \quad (6)$$

$$I_{pa}\ [PANI/ITO]\ (A) = 1.66 \times 10^{-5} \times v^{1/2} + 5.6315 \times 10^{-5};\ R^2 = 0.9905 \quad (7)$$

$$I_{pc}\ [PANI/ITO]\ (A) = -9.31 \times 10^{-6} \times v^{1/2} - 6.422 \times 10^{-5};\ R^2 = 0.9855 \quad (8)$$

The value of electron transfer co-efficient (α) for both PANI and PANI@CeO_2 grafted ITO electrodes was obtained to be 0.9138 and 0.8874, respectively (Equation S1). Using the value of (α) and the Equation (S2), the value of the charge transfer rate constant (K_s) is found to be 0.1804 s^{-1} and 0.8185 s^{-1} for PANI and PANI@CeO_2 respectively. Further, the value of average surface coverage (λ) is to be calculated using Equation S3, which is found to be 1.515×10^{-4} m^{-2} and 2.07×10^{-4} m^{-2} for PANI and PANI@CeO_2 respectively. The value of diffusion coefficient for $[Fe(CN)_6]^{3-/4-}$ solution (D) and effective surface area of electrodes (A) are calculated using the gradient of lines established by the linear connection between I_p and $v^{1/2}$, using the Randles-Sevcik equation as shown in Equation (S4).

The effective surface area of PANI having $D = 4.964 \times 10^{-4}$ m^2 s^{-1} and PANI@CeO_2 having $D = 9.5 \times 10^{-4}$ m^2 s^{-1} is found to be 5.22×10^{-7} m^2 and 6.32×10^{-7} m^2 respectively. The values of D and A are greater for PANI@CeO_2 nanocomposite than PANI because PANI@CeO_2 performs better diffusion of redox ions through its active detection area and electrode interface [26,27]. All the parameters have been summarized in **Table 1**.

Table 1. Comparison of the electrochemical behaviour of the PANI/ITO and PANI@CeO_2/ITO electrodes.

Modified electrodes	Electron transfer co-efficient (α)	Charge transfer rate constant (K_s) (s^{-1})	Average surface coverage (λ) (m^{-2})	Diffusion co-efficient (D) (m^2s^{-1})	Effective surface area (A) (m^2)
PANI/ITO	0.9138	0.1804	1.515×10^{-4}	4.964×10^{-4}	5.22×10^{-7}
PANI@CeO_2/ITO	0.8874	0.8184	2.07×10^{-4}	9.5×10^{-4}	6.32×10^{-7}

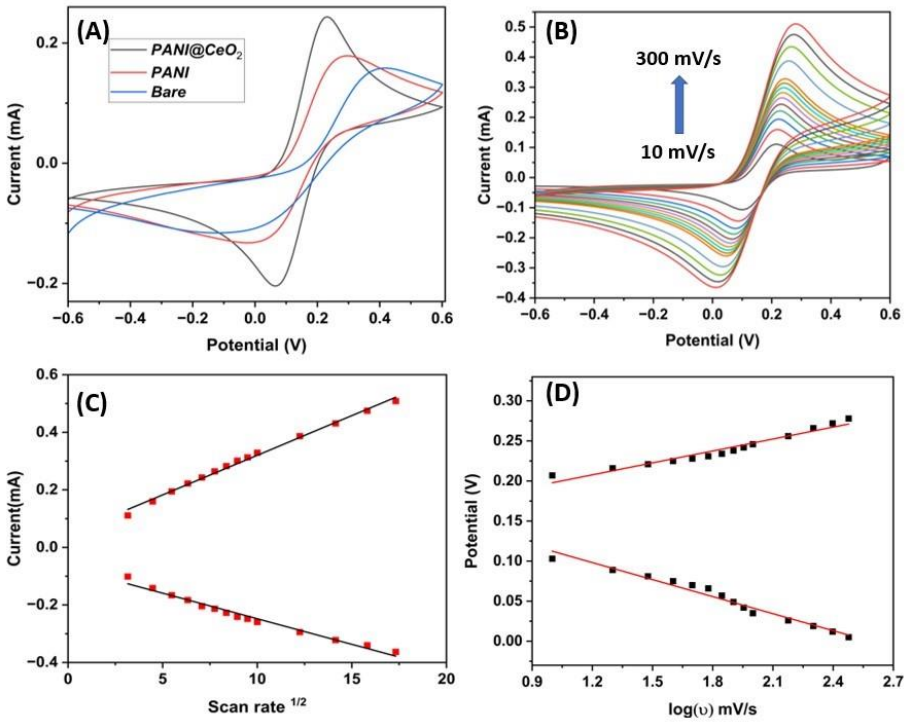

Figure 4. (A) CV studies of PANI@CeO_2, PANI and bare electrode demonstrating the higher conduction ability of PANI@CeO_2; **(B)** different scan rates with PANI@CeO_2 electrode (10–300 mV/s); **(C)** Plot of I_{pa}, I_{pc} vs. square root of scan rate for PANI@CeO_2 electrode; **(D)** plot of potential vs. logarithm of scan rate for pani@CeO_2 electrode.

4.2. Optimization of pH parameter

For an effective sensing methodology of the electrodes, it is mandatory to optimize the value of pH of the electrolyte solution, as the pH affects the sensitivity of the electrode towards the analyte. Thus, we performed the optimization of buffer solution from pH 5.5 to pH 8.5 using the DPV. Maximum current has been observed at pH 7.4, and thus we used pH 7.4 buffer for all the sensing studies (**Figure S4**). This can be attributed to the fact that the rate of deprotonation of phenols declines with the rise in pH of the solution. Also, human body serum has an optimum pH of 7.4, hence this pH is favourable for clinical studies as well [8].

4.3. Electrochemical biosensing of E2

The electrochemical sensing of E2 was performed using the DPV technique in PBS (pH 7.4) carrying 5 mM $[Fe(CN)_6]^{-3/-4}$ solution, as shown in **Figure 5A**. It was noticed that the peak current declined linearly with the concentration of the E2 as analyte (1–100 μM). This can be justified as, with an increase in concentration, the analyte tends to bind with iron coming from $[Fe(CN)_6]^{-3/-4}$ solution to make an iron complex, which retards the analyte from getting onto the electrode surface of the

PANI@CeO_2 modified ITO electrode [28]. The linear correlation between the concentration and peak current of the analyte is illustrated in **Figure 5B**, which follows the equation:

$$I\,(A) = 7.6 \times 10^{-5} - 9.012 \times 10^{-8}\,[\text{E2}];\ R^2 = 0.9865$$

From the slope of the equation, the sensitivity of the biosensor obtained is 142.6 μA μM^{-1} m^{-2}. The fabricated electrode offers an LOD of 21.53 μM towards E2 with reference to the equation: LOD = $3\sigma/S$. (σ = standard deviation, S = sensitivity, which is determined from the slope of the calibration curve) [29]. The aromatic ring of E2 consists of the hydroxy group, which is liable to make phenoxyl radicals in an aqueous medium during the process of oxidation. The radical on further oxidation leads to the formation of commensurate ketone derivatives, which conclude the effective electrocatalytic direct oxidation of E2 using PANI@CeO_2 [30].

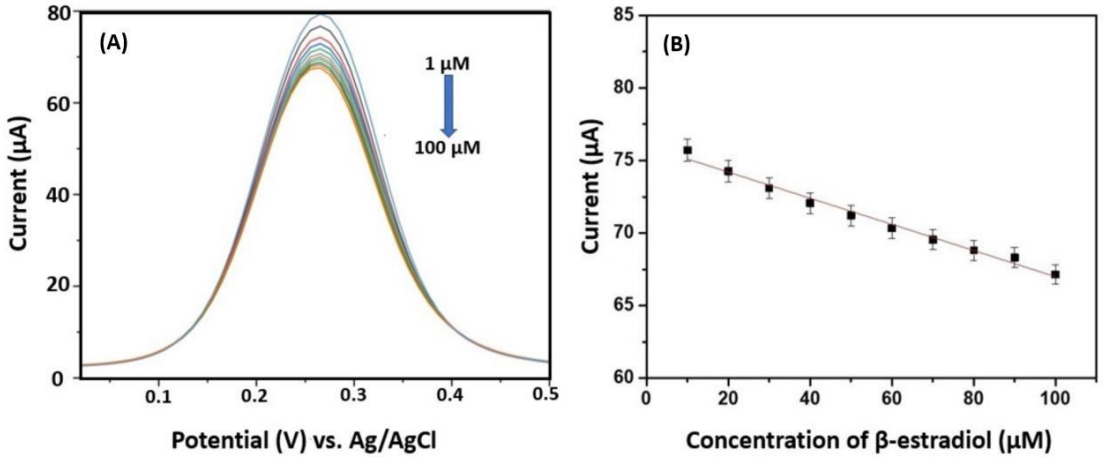

Figure 5. (A) DPV response for PANI@CeO_2 electrode with increase in concentration of E2 as an analyte (1–100 μM); **(B)** Calibration plot between magnitude of current response vs. Concentration of the analyte where linearity is observed.

4.4. Interference, shelf life and stability study

To understand the specificity for analyte E2, an interference study has been performed by testing E2 (100 μM) in the presence of equal amounts of interferants like ascorbic acid (100 μM), glucose, NaCl, urea, estriol, and uric acid, which might restrict the sensing of E2 while its detection in urine and water samples. It has been observed from the current response for different interferants that the target analyte maintained its specificity in different interferants (**Figure 6A**).

Further, the shelf life of the developed electrode was examined for 21 days in the interval of 7 days. From this study, no change in the current response is observed till 14 days. Whereas a sudden diminution in peak current of around 12.1% is noticed on the 21st day of this study. Therefore, we confirm the good stability of the developed biosensor for a period of up to 15 days (**Figure 6B**). However, the stability of the biosensing electrode has been confirmed by repeating each result thrice.

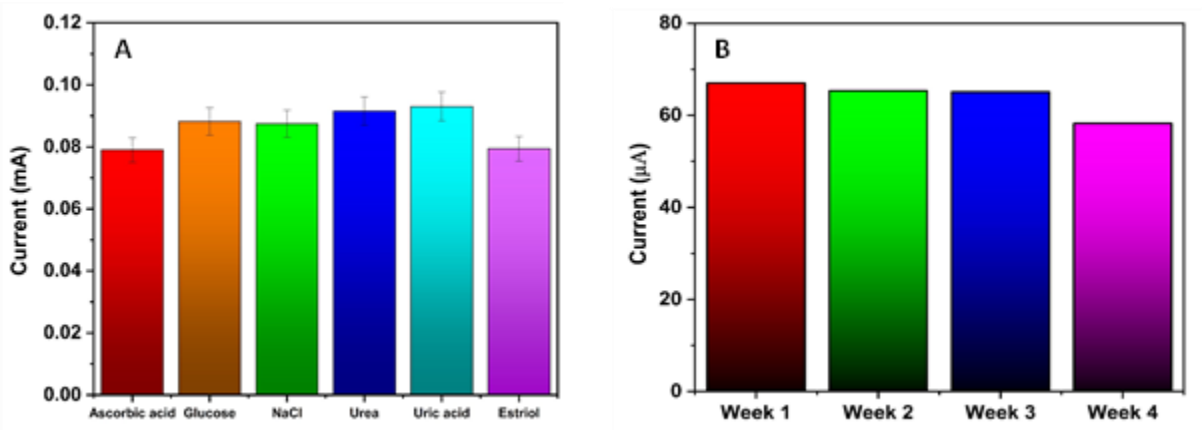

Figure 6. (A) Interference study for different analytes indicating the specificity of E2 analyte; **(B)** Shelf study of the PANI@CeO_2 modified electrode in 7.4 pH PBS containing 5 mM $[Fe(CN)_6]^{3-/4-}$ for 100 µM E2; from this result, we confirmed a shelf life of up to 15 days for the developed biosensor.

4.5. Real sample analysis

To examine the precision and practical applicability of our biosensor, we performed electrochemical analysis in two different samples, viz., human urine (healthy female) and tap water (DTU, Delhi). For analysis, each real sample was infused with different concentrations of E2 (1–100 µM) [31]. From the above analysis, we observed recovery of E2 in the range of 98.3%–99.7% for human urine and 97.1%–98.1% for tap water which validates the good productivity and effectuality of the PANI@CeO_2 electrode (**Table 2**).

Table 2. Recovery percentage data of E2 in real samples.

Sample	Added amount (µM)	Found amount (µM)	Recovery (%)
Human urine	10	9.85	98.5
	40	39.88	99.7
	60	59.64	99.4
	100	98.3	98.3
Tap water	10	9.71	97.1
	40	38.92	97.3
	60	58.86	98.1
	100	97.6	97.6

5. Conclusion

In this study, a method was incorporated to detect E2 using a non-enzymatic approach. We synthesized and characterized a PANI@CeO_2 nanocomposite, which was then electrophoretically deposited onto an ITO substrate. The electrochemical behaviour of the PANI@CeO_2 modified electrode was compared to a PANI modified electrode.

After considering the results, this work can be summarized as:

a) The incorporation of CeO_2 in the conducting polymer (PANI), forming PANI@CeO_2 acts as an effective sensing platform for E2. PANI matrix grafted

with CeO_2 increases the surface area, density, electrical conductivity, and sensitivity of nanocomposite.

b) PANI@CeO_2 modified electrode persisting higher current as compared to PANI modified electrode has been depicted, indicating better diffusion of redox ions.

c) The study also included a quantitative analysis of three important parameters: sensitivity (275.4 mA $(\mu M)^{-1}$), linear range (1–100 μM), and limit of detection (2.15 μM). These results demonstrated the reliability and performance of the developed biosensor in terms of sensitivity, range, and detection limit. The experiments showed good repeatability, stability, and reproducibility, further validating the effectiveness of the non-enzymatic biosensor for detecting E2.

d) For better evaluation, the applicability of the biosensor is demonstrated by conducting the analysis in real samples, viz., human urine and tap water, which showcase the practicality and potential of the biosensor in real-world scenarios.

Supplementary materials: Consists of supporting equations, XRD and FTIR pattern of PANI, and pH optimization results.

Author contributions: Conceptualization, AD, and TR; methodology, SV; software, AD; validation, SV and DK; formal analysis, SV; investigation, AD and TR; resources, AD; data curation, TR; writing—original draft preparation, AD and TR; writing—review and editing, SV; visualization, SV; supervision, DK. All authors have read and agreed to the published version of the manuscript.

Funding: Authors thank Dept. of Physics, DTU, Delhi India for the XRD facility. S. Verma acknowledges UGC for the JRF Award (NOV 2017-139082).

Data availability: The data that has been used is confidential.

Conflict of interest: The authors declare no conflict of interest.

References

1. Wang Y, Zhao X, Zhang M, et al. A fluorescent amplification strategy for high-sensitive detection of 17 β-estradiol based on EXPAR and HCR. Analytica Chimica Acta. 2020; 1116: 1-8. doi: 10.1016/j.aca.2020.04.010
2. Pu H, Huang Z, Sun DW, et al. Recent advances in the detection of 17β-estradiol in food matrices: A review. Critical Reviews in Food Science and Nutrition. 2019; 59(13): 2144-2157. doi: 10.1080/10408398.2019.1611539
3. Orozco-Hernández L, Gómez-Oliván LM, Elizalde-Velázquez A, et al. 17-β-Estradiol: Significant reduction of its toxicity in water treated by photocatalysis. Science of The Total Environment. 2019; 669: 955-963. doi: 10.1016/j.scitotenv.2019.03.190
4. Minopoli A, Sakač N, Lenyk B, et al. LSPR-based colorimetric immunosensor for rapid and sensitive 17β-estradiol detection in tap water. Sensors and Actuators B: Chemical. 2020; 308: 127699. doi: 10.1016/j.snb.2020.127699
5. Yao X, Wang Z, Dou L, et al. An innovative immunochromatography assay for highly sensitive detection of 17β-estradiol based on an indirect probe strategy. Sensors and Actuators B: Chemical. 2019; 289: 48-55. doi: 10.1016/j.snb.2019.03.078
6. Triviño JJ, Gómez M, Valenzuela J, et al. Determination of a natural (17β-estradiol) and a synthetic (17α-ethinylestradiol) hormones in pharmaceutical formulations and urine by adsorptive stripping voltammetry. Sensors and Actuators B: Chemical. 2019; 297: 126728. doi: 10.1016/j.snb.2019.126728
7. Goswami B, Mahanta D. Fe3O4-Polyaniline Nanocomposite for Non-enzymatic Electrochemical Detection of 2,4-Dichlorophenoxyacetic Acid. ACS Omega. 2021; 6(27): 17239-17246. doi: 10.1021/acsomega.1c00983
8. Paneru S, Kumar D. A Novel Electrochemical Biosensor Based on Polyaniline-Embedded Copper Oxide Nanoparticles for High-Sensitive Paraoxon-Ethyl (PE) Detection. Applied Biochemistry and Biotechnology. 2023; 195(7): 4485-4502. doi: 10.1007/s12010-023-04350-y

9. Ramanavicius S, Ramanavicius A. Conducting Polymers in the Design of Biosensors and Biofuel Cells. Polymers. 2020; 13(1): 49. doi: 10.3390/polym13010049
10. Petruleviciene M, Juodkazyte J, Savickaja I, et al. BiVO4-based coatings for non-enzymatic photoelectrochemical glucose determination. Journal of Electroanalytical Chemistry. 2022; 918: 116446. doi: 10.1016/j.jelechem.2022.116446
11. Emir G, Dilgin Y, Ramanaviciene A, et al. Amperometric nonenzymatic glucose biosensor based on graphite rod electrode modified by Ni-nanoparticle/polypyrrole composite. Microchemical Journal. 2021; 161: 105751. doi: 10.1016/j.microc.2020.105751
12. Adeosun WA, Asiri AM, Marwani HM, et al. Enzymeless Electrocatalytic Detection of Uric Acid Using Polydopamine/Polypyrrole Copolymeric film. ChemistrySelect. 2020; 5(1): 156-164. doi: 10.1002/slct.201903628
13. Ashwini IS, Pattar J, Anjaneyulu P, et al. Synthesis and electrical properties of polyaniline–cerium oxide composites. Synthetic Metals. 2020; 270: 116588. doi: 10.1016/j.synthmet.2020.116588
14. Rossignatti BC, Vieira AP, Barbosa MS, et al. Thin Films of Polyaniline-Based Nanocomposites with CeO2 and WO3 Metal Oxides Applied to the Impedimetric and Capacitive Transducer Stages in Chemical Sensors. Polymers. 2023; 15(3): 578. doi: 10.3390/polym15030578
15. Sharma SS, Palatty S. Advances in functionalized polyaniline nanocomposites for electrochemical sensing and energy storage applications. Applications of Multifunctional Nanomaterials. 2023; 2023: 177-196. doi: 10.1016/b978-0-12-820557-0.00004-7
16. Beygisangchin M, Abdul Rashid S, Shafie S, et al. Preparations, Properties, and Applications of Polyaniline and Polyaniline Thin Films—A Review. Polymers. 2021; 13(12): 2003. doi: 10.3390/polym13122003
17. Hussein MA, Khan A, Alamry KA. A highly efficient electrochemical sensor containing polyaniline/cerium oxide nanocomposites for hydrogen peroxide detection. RSC Advances. 2022; 12(49): 31506-31517. doi: 10.1039/d2ra05041b
18. Lei Y, Qiu Z, Tan N, et al. Polyaniline/CeO2 nanocomposites as corrosion inhibitors for improving the corrosive performance of epoxy coating on carbon steel in 3.5% NaCl solution. Progress in Organic Coatings. 2020; 139: 105430. doi: 10.1016/j.porgcoat.2019.105430
19. Parvatikar N, Jain S, Bhoraskar SV, et al. Spectroscopic and electrical properties of polyaniline/CeO2 composites and their application as humidity sensor. Journal of Applied Polymer Science. 2006; 102(6): 5533-5537. doi: 10.1002/app.24636
20. Li C, Wang J, Wen Y, et al. Polyaniline/CeO2 Nanofiber Composite Membrane as a Promoter of Pt for Formic Acid Electro-Oxidation. ECS Electrochemistry Letters. 2012; 2(1): H1-H4. doi: 10.1149/2.001302eel
21. Saranya J, Sreeja BS, Padmalaya G, et al. Ultrasonic Assisted Cerium Oxide/Graphene Oxide Hybrid: Preparation, Anti-proliferative, Apoptotic Induction and G2/M Cell Cycle Arrest in HeLa Cell Lines. Journal of Inorganic and Organometallic Polymers and Materials. 2020; 30(7): 2666-2676. doi: 10.1007/s10904-019-01403-w
22. Huang H, Guo ZC. Preparation and Characterization of Conductive Polyaniline/Cerium Dioxide Composites. Materials Science Forum. 2010; 663-665: 686-689. doi: 10.4028/www.scientific.net/msf.663-665.686
23. Wang S, Huang Z, Wang J, et al. Thermal stability of several polyaniline/rare earth oxide composites (I): polyaniline/CeO2 composites. Journal of Thermal Analysis and Calorimetry. 2011; 107(3): 1199-1203. doi: 10.1007/s10973-011-1777-1
24. Ramezanzadeh B, Bahlakeh G, Ramezanzadeh M. Polyaniline-cerium oxide (PAni-CeO2) coated graphene oxide for enhancement of epoxy coating corrosion protection performance on mild steel. Corrosion Science. 2018; 137: 111-126. doi: 10.1016/j.corsci.2018.03.038
25. Elgrishi N, Rountree KJ, McCarthy BD, et al. A Practical Beginner's Guide to Cyclic Voltammetry. Journal of Chemical Education. 2018; 95(2): 197-206. doi: 10.1021/acs.jchemed.7b00361
26. Laviron E. General expression of the linear potential sweep voltammogram in the case of diffusionless electrochemical systems. Journal of Electroanalytical Chemistry and Interfacial Electrochemistry. 1979; 101: 19-28. doi: 10.1016/S0022-0728(79)80075-3
27. Jalil O, Pandey CM, Kumar D. Highly sensitive electrochemical detection of cancer biomarker based on anti-EpCAM conjugated molybdenum disulfide grafted reduced graphene oxide nanohybrid. Bioelectrochemistry. 2021; 138: 107733. doi: 10.1016/j.bioelechem.2020.107733
28. Li J, Liu S, Yu J, et al. Electrochemical immunosensor based on graphene-polyaniline composites and carboxylated graphene oxide for estradiol detection. Sensors and Actuators B: Chemical. 2013; 188: 99-105. doi: 10.1016/j.snb.2013.06.082

29. Verma S, Pandey CM, Kumar D. A highly efficient rGO grafted MoS2 nanocomposite for dye adsorption and electrochemical detection of hydroquinone in wastewater. New Journal of Chemistry. 2022; 46(44): 21190-21200. doi: 10.1039/d2nj04285a
30. Li J, Jiang J, Zhao D, et al. Facile synthesis of Pd/N-doped reduced graphene oxide via a moderate wet-chemical route for non-enzymatic electrochemical detection of estradiol. Journal of Alloys and Compounds. 2018; 769: 566-575. doi: 10.1016/j.jallcom.2018.08.016
31. Supchocksoonthorn P, Alvior Sinoy MC, de Luna MDG, et al. Facile fabrication of 17β-estradiol electrochemical sensor using polyaniline/carbon dot-coated glassy carbon electrode with synergistically enhanced electrochemical stability. Talanta. 2021; 235: 122782. doi: 10.1016/j.talanta.2021.122782